JOURNAL OF PROPULSION AND POWER
Vol. 9, No. 6, Nov.–Dec. 1993

Airfoil Wake and Linear Theory Gust Response Including Sub- and Superresonant Flow Conditions

Gregory H. Henderson* and Sanford Fleeter†
Purdue University, West Lafayette, Indiana 47907

The unsteady aerodynamic gust response of a high solidity stator vane row including the effects near an acoustic resonance are investigated experimentally for the first time. This is accomplished by means of a series of experiments performed in the Purdue Annular Cascade Research Facility, with gusts generated by rotors comprised of perforated plates and airfoils. The perforated-plate generated forcing functions closely resemble linear-theory vortical gusts. However, the airfoil wake generated forcing functions are much more complex and exhibit characteristics far from linear-theory vortical gusts. The response of the instrumented symmetric airfoil stator vane row to the linear theory gusts are in excellent agreement with linear theory predictions for experimental conditions not in the immediate neighborhood of an acoustic resonance. The response of the stator vane cascade to airfoil-cascade forcing functions correlates poorly with linear-theory gust predictions, with the unsteady lift and moment coefficients controlled by the characteristics of the forcing function. For both the perforated plate and airfoil wake generated gusts, the unsteady pressure responses do not agree with the linear-theory gust predictions near an acoustic resonance, but the effects of the acoustic resonance phenomena are clearly evident on the airfoil surface unsteady pressure responses. The transition of the measured lift coefficients across the acoustic resonance from the subresonant regime to the superresonant regime occurs in a simple linear fashion.

Nomenclature

C = stator airfoil chord length
$\bar{C}_p$ = steady surface pressure coefficient
$\bar{C}_{\Delta p}$ = steady differential pressure coefficient
$\tilde{C}_p$ = unsteady surface pressure coefficient
$\tilde{C}_{\Delta p}$ = unsteady differential pressure coefficient
$\boldsymbol{k}$ = gust propagation wave number vector
k_b = reduced frequency based on semichord
k_c = reduced frequency based on chord
S = airfoil spacing
U = absolute velocity
u^+ = streamwise gust amplitude
v^+ = transverse gust amplitude
W = relative velocity
W_p = plate width
$\bar{W}_1$ = inlet mean-relative velocity
$\bar{W}_2$ = rotor exit mean relative velocity
w^+ = gust amplitude
α = angle of attack
$\bar{\alpha}_1$ = rotor inlet mean absolute flow direction
$\bar{\alpha}_2$ = rotor exit mean absolute flow direction
β_w = gust amplitude angle
β'_w = gust velocity vector angle
$\bar{\beta}_1$ = rotor inlet mean-relative flow angle
$\bar{\beta}_2$ = rotor exit mean-relative flow angle
ρ_0 = freestream density
σ = interblade phase angle
σ_r = resonant interblade phase angle $\geq\geq\geq$
Ω = rotor velocity
Ω_f = free-rotation rotor velocity
ϕ_w = gust component phase angle

Presented as Paper 92-3074 at the AIAA/SAE/ASME/ASEE 28th Joint Propulsion Conference, Nashville, TN, July 6–8, 1992; received Oct. 21, 1992; revision received May 5, 1993; accepted for publication May 10, 1993.

*School of Mechanical Engineering; currently Senior Engineer, Advanced Heavy Duty Performance at Cummins Engine Company, Advanced Product Development, Columbus, IN 47203.

†Professor, School of Mechanical Engineering. Associate Fellow AIAA.

Introduction

AERODYNAMICALLY induced structural failures of blade components pose significant problems in the development of turbomachines. Dynamic blade stresses result from the transfer of energy from the flowfield to blade motion and strain energy. The cumulative effects of repetitive vibratory stresses lead to fatigue failure in blade materials. Finite element techniques accurately predict the blade structural characteristics. However, specifying the blade row unsteady aerodynamic loading has not reached the same predictive capabilities.

In a multistage turbomachine, downstream blade rows are periodically in the wakes generated by upstream airfoils. As a result, the inlet flowfield to the downstream blade row varies periodically with time. Such blade-row-wake interactions are the most common and least understood source of unsteady aerodynamic excitation causing high-cycle blade fatigue. The a priori prediction of flow-induced vibration stresses cannot be made with current technology due to the inadequacy of unsteady aerodynamic models. Thus, costly redesigns are necessary when engine development testing reveals unacceptable blade stress levels.

Blade row vibratory response induced by the relative motion of adjacent blade row wake and potential field flows is termed forced response. The forced response unsteady aerodynamics problem is often simplified by assuming linear superposition of two types of blade unsteady aerodynamic loadings: 1) the aerodynamic forcing function response results from the interaction of rigid blade-rows with wakes; and 2) motion-induced unsteady aerodynamic response or aerodynamic damping results when the blade row undergoes harmonic motion. This article is focused upon the aerodynamic forcing function response.

State-of-the-art unsteady aerodynamic analyses are essentially limited to two-dimensional linearized perfect-fluid theory models. In the absolute reference frame, the steady flow past flat plate airfoil cascades is uniform, with a small perturbation unsteady flow resulting from the upstream rotor

blade wake flowfield resolved into streamwise and transverse components. Advanced analyses which allow the potential field of the downstream airfoils to distort the wake by linearizing about the nonuniform mean flow near the blade row, instead of the much simpler upstream uniform mean flow, are currently being developed.[1-3] In all of these models, the wake is defined in terms of its harmonics, with each harmonic forcing function modeled as a gust forcing function boundary condition in the prediction of the resulting blade row unsteady aerodynamics. Thus, even though forcing functions can be generated by a wide variety of fundamentally different phenomena, all forcing functions are modeled as being equivalent, with the resulting predicted blade row response independent of the particular wake generator.

A number of experiments have been directed at the verification of unsteady aerodynamic models appropriate for blade row forced response prediction and the determination of their applicability and limitations.[4-9] In these, the unsteady airfoil row response comparisons with linear theory were made without considering the fundamental gust modeling assumptions. However, it has been found experimentally that the harmonic gust response generated by different—but equivalent—forcing functions are dependent on the particular forcing function.[10,11] Also, the fundamental gust modeling assumption for a very low solidity symmetric airfoil cascade has been investigated.[12,13] These data quantitatively showed that airfoil wakes are not able to be modeled with the vortical gust boundary conditions of current state-of-the-art linear unsteady aerodynamic theory, with the forcing function generator significantly affecting the resulting gust response.

In this article, the unsteady aerodynamic gust response of a high solidity stator vane row, including the effects of operating in the subresonant and superresonant flow regimes, i.e., acoustic resonances, are investigated experimentally in terms of the fundamental gust modeling assumptions for the first time. Therefore, these high solidity cambered airfoil data are of direct interest to turbomachine designers, with these unique data significantly extending previous results. This is accomplished by means of a series of experiments performed in the Purdue Annular Cascade Research Facility. Linear theory gust forcing functions are generated by a rotating row of perforated plates, with the compressor and turbine blade wakes associated with a rotor blade row. The stator vane row is comprised of instrumented symmetric airfoils.

Linear Theory Gust Characteristics

In classical linear perfect-fluid theory, the wake flowfield is composed of a uniform mean flow and a superimposed sinusoidal vortical gust w propagating according to k. The resulting blade-row flowfield schematic is presented in Fig. 1.

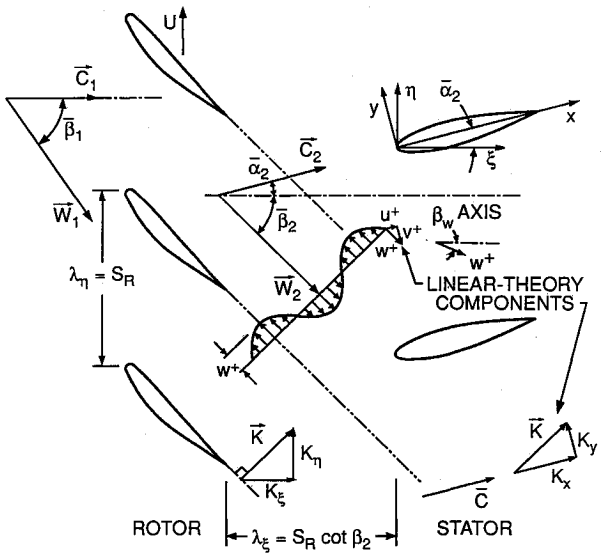

Fig. 1 Turbomachine gust propagation.

In the stationary reference frame of a downstream airfoil row, the propagation of the harmonic wake velocity field is defined by considering periodicity requirements in the axial-circumferential coordinate system. As a consequence of this periodicity, the downstream mean-relative flow W_2 and k are perpendicular.

The stator row flowfield is modeled as being compressible and isentropic, and is analyzed by superpositioning of rotational and irrotational flowfields which satisfy continuity independently.[14] The unsteady aerodynamic loads on an airfoil are determined by solving the velocity potential equation using standard techniques subject to the Kutta condition and the solid boundary condition at the airfoil surface. The flowfield pressure distribution is obtained by integrating the linearized Bernoulli Equation with the known velocity potential.

Two constraints are imposed by continuity on the downstream rotational forcing function wake flowfield. The primary constraint is the requirement that ϕ_w be either 0 or 180 deg. If this primary constraint is satisfied, then the secondary constraint stipulates that the gust-component amplitude vector must be parallel to the downstream mean-relative flow $w^+ \| W_2$. When the primary constraint is satisfied, the gust amplitude simplifies to $w^+ = \sqrt{u^{+2} + v^{+2}}$, with the periodic velocity vectors parallel over the entire periodic cycle.

Gust profiles are completely defined by specifying k, w^+, β_w, and ϕ_w. If the primary gust constraint is violated, β_w is distinct from β'_w, the angle of any velocity vector, and w^+ is not equal to $\sqrt{u^{+2} + v^{+2}}$. Note that β'_w is the angle of any velocity vector and varies with time and space, whereas β_w is the angle of the maximum gust magnitude or gust amplitude w^+, and is a constant. For a gust that violates the primary constraint, the gust amplitude and gust-amplitude angle are found by maximizing the velocity vector magnitude.

Acoustic Resonance

Linear subsonic compressible cascade theory predicts the existence of pressure waves emanating from the airfoil surfaces and propagating in two modes. When pressure disturbances propagate away from the cascade unattenuated, the flowfield is superresonant. The flowfield is subresonant when the pressure waves are attenuated exponentially with distance from the cascade. These two regimes are separated by the acoustic resonance condition.

Forced response acoustic resonance conditions are related to the cascade σ, a constant which describes the unsteady aerodynamics between adjacent blades. It is specified by the ratio of the number of upstream blades to the number of downstream blades

$$\sigma = -2\pi \frac{N_{\text{upstream}}}{N_{\text{downstream}}} \pm 2\pi l \tag{1}$$

where the parameter l is any integer value which puts σ in the desired range.

An expression for σ_r has been derived[15] and presented here as Eq. (2). This equation specifies two resonant interblade phase angles, σ_r^- and σ_r^+, which are associated with the sign in the denominator. Figure 2 illustrates subsonic cascade behavior in terms of the wave propagation regimes. The positive and negative resonant interblade phase angles bracket the superresonant regime which always includes $\sigma = 0$, with the acoustic regimes repeating with a period of 2π. For a flat plate cascade in a subsonic mean flow, the resonant interblade phase angles are given by the following:

$$\sigma_r = \frac{k_c M(S/C)}{\sqrt{1 - M^2 \sin^2\gamma} \pm M \cos\gamma} \pm 2\pi l \tag{2}$$

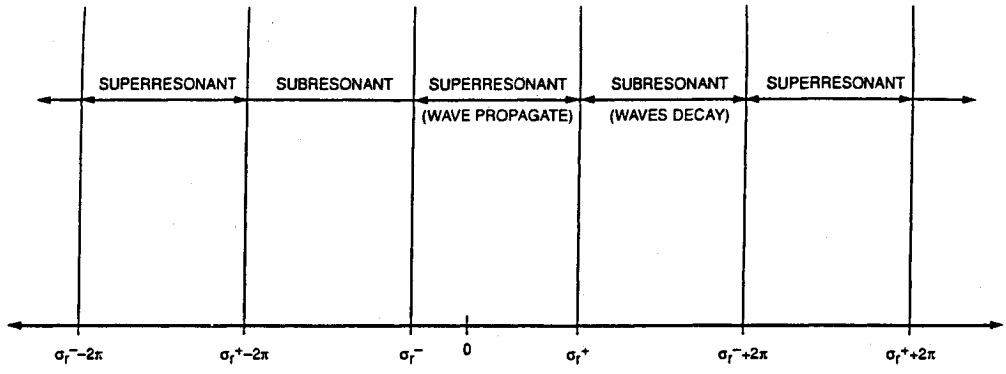

Fig. 2 Regimes of pressure wave propagation.

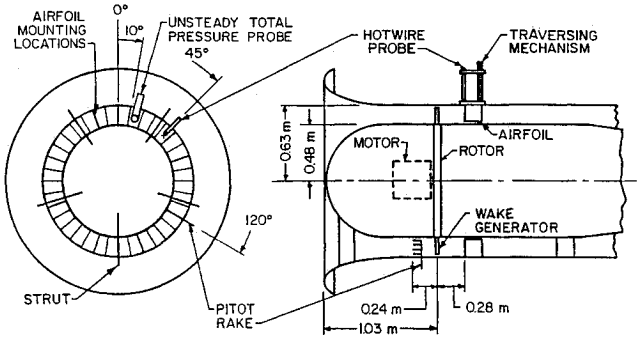

Fig. 3 Test section schematic.

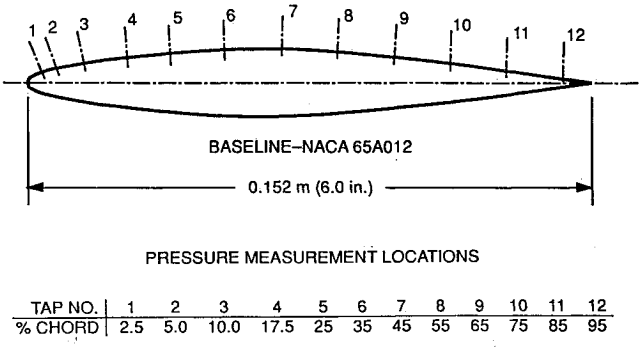

TAP NO.	1	2	3	4	5	6	7	8	9	10	11	12
% CHORD	2.5	5.0	10.0	17.5	25	35	45	55	65	75	85	95

Fig. 4 Instrumented stator airfoil profile.

where γ is the stagger angle, M is the Mach number, and C/S is the cascade solidity.

Research Facility

The Purdue Annular Cascade Research Facility is an open-loop draw-through type wind tunnel, capable of test section velocities of 70 m/s (220 ft/s). The inlet flow, conditioned first by a honeycomb section and then a settling chamber, accelerates into the annular test section via a bellmouth inlet. The test section exit flow is diffused into a large plenum. The 224-kW (300-hp) centrifugal fan located downstream of the plenum draws the air through the facility, with the guide vanes at the fan inlet allowing flow rate adjustment through the facility. The annular test section (Fig. 3) houses a rotor independently driven by a 7.5-kW (10-hp) A-C motor controlled by a variable frequency drive to create the desired unsteady flowfield together with a downstream stator row. The separate drive motors on the rotor and system fan uncoupled the rotor speed from the through-flow velocity. Thus, independent control over unsteady aerodynamic parameters, i.e., the reduced frequency, is possible since the system flow rate is independent of the rotor speed and rotor configuration.

Stator Vane Row

Figure 4 presents the symmetric NACA 65A012 stator airfoil profile. The airfoil chord and span are equal at 0.152 m (6.0 in.). This stator cascade is comprised of 18 airfoils, resulting in a solidity of 0.78. The 12 chordwise instrumentation locations shown in Fig. 4 provide highly detailed spatial resolution of the midspan chordwise steady and unsteady pressure distributions. These high solidity stator cascade experiments were conducted with 20 wake generators, with the rotor speed setting used to adjust the reduced frequency. Also, it should be noted that an acoustic resonance is predicted by linear theory within the operating range of the facility for this ratio of the number of wake generators to stator airfoils.

Data Acquisition and Analysis

The unsteady data defining the gust forcing function are determined from the unsteady velocity and static pressure fluctuations. The rotor-exit flowfield unsteady total pressure is measured with a total pressure pitot tube fitted with an unsteady pressure transducer. A cross hot-wire anemometer located on the downstream stator vane row leading-edge line is used to measure the stator cascade inlet flowfield.

Static pressure taps and high-response pressure transducers embedded in the stators are used to obtain the detailed airfoil-surface steady and unsteady pressure data. Four instrumented airfoils are required, two to obtain static pressure distributions on each airfoil surface and two to obtain the periodic pressure distributions on each surface.

The stator-cascade steady and unsteady velocity fields are measured with the cross hot-wire probe, with these measured wake velocity deficits then decomposed into streamwise and transverse components. The estimated uncertainties of the velocity magnitude and direction are $\pm 5\%$ and ± 1 deg, respectively. The total pressure fluctuations downstream of the rotor are measured with the unsteady total pressure probe, with the static pressure distributions calculated by subtracting the dynamic pressure $\rho_0 \bar{U}_2^2/2$ from the total pressure.

The stator vane row airfoil unsteady surface pressures are measured with PCB Piezotronics model 103A piezoelectric pressure transducers. The transducers have a nominal sensitivity of 0.22 mV/Pa (1500 mV/psi), and a natural frequency of 13 kHz. The estimated uncertainty of the unsteady pressure measurements is $\pm 3\%$. After the transducers were installed in the airfoil, the dynamic response of each airfoil transducer-passage system was experimentally determined to correct for any passage effects.

The time variant signals are digitized over one rotor revolution using approximately 2000 samples. Ensemble-averaging the hot-wire and pressure transducer signals 150 and 100 times, respectively, produces very clean periodic time traces with the random fluctuations averaged away. The Fourier components of the ensemble-averaged time traces are

numerically determined with fast Fourier transform software. The sample frequency is set and the number of samples is adjusted to produce time records of exactly one rotor rotation period to eliminate frequency leakage problems in Fourier transform analysis.

The stator vane chordwise unsteady pressure response data are correlated with a compressible flow analysis which accounts for the cascade stagger angle γ, solidity C/S, reduced frequency k_c, and σ.[16] This linear analysis assumes subsonic, inviscid two-dimensional flow past flat plate airfoil cascades.

The unsteady periodic signals are Fourier decomposed and each pressure harmonic nondimensionalized by calculating an unsteady surface pressure coefficient

$$\hat{C}_p(x) = \frac{\hat{p}(x)}{\rho \bar{U} \hat{v}} \tag{3}$$

where $\hat{p}$ and $\hat{v}$ represent the harmonic surface pressure and transverse gust component, respectively.

The harmonic differential pressure coefficient is defined by

$$\hat{C}_{\Delta p} = \hat{C}_{p,l} - \hat{C}_{p,u} \tag{4}$$

Direct comparison of the experimental and theoretical unsteady lift coefficients is accomplished by integrating the experimental and theoretical chordwise differential pressure coefficients over the airfoil chord:

$$C_L = \frac{1}{C} \int_{0.025C}^{0.95C} C_{\Delta p}\, dx \tag{5}$$

The trapezoidal rule is used to evaluate the integral from the discrete differential pressure coefficient data and theoretical predictions. The differential pressure distributions were integrated from the leading-edge tap location, $0.025C$, to the trailing edge tap location, $0.95C$. In a similar manner, experimental and theoretical quarter-chord moment coefficients are calculated.

The complex valued unsteady vane surface pressure data contain both amplitude and phase angle information. These quantities are referenced to the transverse gust sinusoid measured by the cross hot-wire on the airfoil leading-edge plane. To obtain pressure coefficients for a single equivalent airfoil, the pressure signals are phase corrected to account for the circumferential locations of the instrumented airfoils.

Forcing Functions

The unsteady periodic forcing functions are generated with rotating rows of perforated plates and NACA 0024 airfoil cascades, Fig. 5. A constant axial velocity corresponding to a Mach number of 0.15 was maintained in all experiments. The perforated plates were fabricated from 56% porosity aluminum sheet mounted on the rotor such that the plate width was normal to the rotor axis. The airfoils have a 7-deg twist from the hub to the tip to achieve a constant spanwise angle of attack, and are mounted on the rotor at 35% chord and set to stagger angles measurable to within ± 0.5 deg. The twist was necessary to maintain a two-dimensional unsteady flowfield.

A spanwise survey of the stator cascade inlet flowfield, generated independently by eight perforated plates and eight airfoils, was performed to insure proper two-dimensionality. This survey showed excellent two-dimensionality of the time-averaged flowfield for both wake generators. From 20 to 80% span, the absolute velocity magnitude and flow angle were within 2% and 1 deg, respectively, of the midspan value. The perforated plate generated fundamental harmonics were also highly two-dimensional near the midspan, with the gust amplitude within 5% of the midspan value from the 33% to the 67% span. The twisted rotor blades also produced a two-dimensional fundamental harmonic, with the gust amplitude within 5% of the midspan value from 33 to 67% span.

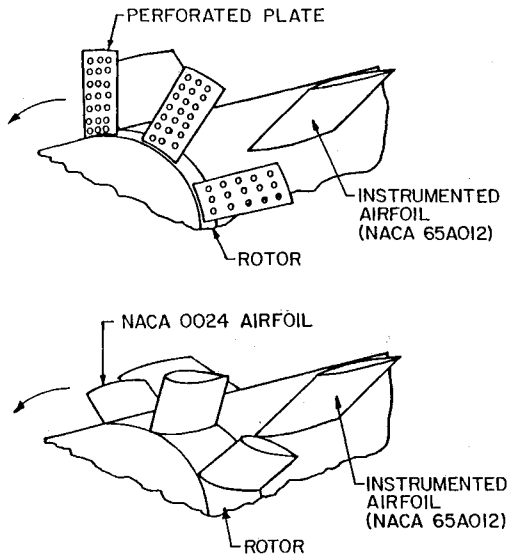

Fig. 5 Forcing function generators.

Fundamental compressor, neutral and turbine rotor forcing functions are generated. This is accomplished by changing the rotor-airfoil steady loading by changing the angle of attack. Three rotor-airfoil angles of attack were investigated, produced by changing the stagger angle while maintaining the same $\bar{\beta}_1$.

For the neutral-loading condition, power to the rotor motor was switched off, allowing the rotor to freely rotate in the flow provided independently by the large downstream centrifugal fan. The friction opposing the rotor rotation is very small, with the rotor mounted directly to the motor shaft which turns in ball bearings. Thus, the only friction producing components in the drive system are the motor ball bearings. A frictionless rotor fitted with flat plate airfoils rotates at the speed required to align the chord line with the inlet mean-relative flow, i.e., the no-load condition. Thus, the stagger angle determines the free-rotation speed in a constant speed flow.

To achieve compressor-loading conditions, the stagger angle was set lower than the neutral-case stagger angle. Power to the drive system was applied to increase the rotor speed to the neutral-load rotor speed. Thus, shaft energy input was required for this rotor loading condition—hence, the description "compressor" loading.

To achieve turbine-loading conditions, the stagger angle was set higher than the neutral-case stagger angle. The rotor motor and speed controller were set to slow the rotor rotation to match the neutral-load rotor speed. Thus, the rotor drive system dissipated energy from the flow, hence, the description "turbine" loading.

The rotor speed ratio Ω_f/Ω, the ratio of the free-rotation rotor speed, i.e., rotor motor off, to the rotor speed under loaded conditions, is used to characterize the degree of rotor loading. This ratio is less than unity for compressor loading since the free-rotation speed is less than the loaded speed, whereas for the turbine-loading condition, the rotor speed ratio is greater than unity. Under all loading conditions, the rotor speed was constant within 0.5%.

Results

To investigate linear theory and compressor, neutral and turbine type wake generated gusts, and the resulting unsteady aerodynamic response of the downstream stator row—including the effects of operating in the subresonant and superresonant flow regimes, i.e., acoustic resonances—a series of

experiments were conducted in the Purdue Annular Cascade Research Facility.

Forcing Functions

A low rotor speed perforated-plate generated aerodynamic forcing function is presented in Fig. 6, obtained with the stator row empty. The periodic velocity vector profile and static pressure distribution define the forcing function. A complete forcing function composed of N_h harmonics is shown together with the forcing function fundamental harmonic. The mean velocity triangles represent the inlet and downstream steady flowfields, denoted by subscripts 1 and 2. The mean velocity triangles include the absolute U, relative W, and rotor Ω velocity vectors normalized by the mean axial velocity, and the absolute and relative flow angles, $\bar{\alpha}$ and $\bar{\beta}$. The inlet flow enters the test section in a purely axial direction. Therefore, the (rotor speed)-to-(axial velocity) ratio determines the inlet mean-relative flow angle $\tan \bar{\beta}_1 = \Omega/\bar{U}_1$. The inlet mean-relative flow angle increases and decreases with rotor speed and is characteristic of the operating point of the facility.

The unsteady velocity vector and static pressure measurements are scaled so that an unsteady velocity vector of unit length represents a velocity pressure fluctuation equal to a unit pressure fluctuation. The velocity and static pressure scale factors, w_{rms} and p_{rms} for small perturbations are linearly related by

$$p_{\text{rms}} = \rho \bar{U}_2 w_{\text{rms}} \tag{6}$$

where w_{rms} is the root-mean-square of the velocity fluctuations and p_{rms} is calculated from Eq. (6). Since w_{rms} and p_{rms} are linearly related by the constant $\rho \bar{U}_2$, scaling in this manner allows the direct determination of the relative proportions of the velocity and static pressure fluctuations.

Linear Gust Forcing Functions

The low rotor speed perforated-plate forcing function presented in Fig. 6 closely resembles a linear-theory vortical gust. In particular, the periodic gust velocity vectors are parallel to W_2, and the static pressure distribution is very small, with the fundamental-harmonic linear gust parameters ϕ_w and β_w very near the linear theory values, with $\phi_w = 182$ deg, and $\beta_w \approx \bar{\beta}_2$.

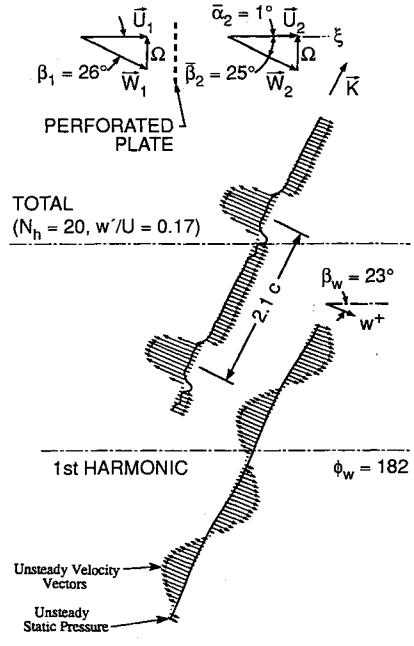

Fig. 6 Low rotor speed perforated plate forcing function.

Perforated-plate fundamental-harmonic linear-gust parameter data β_w and ϕ_w, as a function of rotor solidity and inlet mean-relative flow angle $\beta_w - \bar{\beta}_2$, are presented in Fig. 7. In the upper plots, the difference between the gust-amplitude angle and downstream mean-relative flow angle $\beta_w - \bar{\beta}_2$ is presented. For a linear vortical gust ($\beta_w - \bar{\beta}_2$) is zero. The linear-gust parameters closely match the linear-theory values indicating fundamental-harmonic profiles closely resembling a linear-theory profile. The perforated plates generate linear-theory vortical gust profiles independent of the inlet mean-relative flow angle (i.e., rotor speed) and rotor solidity.

Airfoil-Cascade Forcing Functions

Low-solidity airfoil-cascade forcing functions illustrating the effects of steady rotor loading are presented in Figs. 8–10. Three rotor-airfoil angles of attack corresponding to compressor, neutral, and turbine loading were investigated, produced by changing the stagger angle while maintaining the same $\bar{\beta}_1$.

These forcing functions show gust characteristics far from linear-theory vortical gusts. Not only are the wake region velocity vectors misaligned with the downstream mean-relative flow $\bar{\beta}_2$, the freestream velocity vectors are nonparallel and misaligned with the downstream mean-relative flow. In contrast, the perforated-plate freestream velocity vectors were parallel to $\bar{\beta}_2$. Also, the airfoil forcing functions exhibit sizable static pressure fluctuations which are not considered in the vorticity field of linear theory gusts and are not present in the perforated-plate forcing functions.

The wake-region velocity vectors respond to the rotor loading condition by slanting in the direction of the lift force. The lift force is directed normal to the inlet mean-relative flow, and under compressor-loading conditions pushes on the fluid in the general direction of the gust propagation direction. Under turbine-loading conditions the airfoil pushes on the fluid in the opposite direction, since the lift force has reversed direction 180 deg due to the change in sign of the rotor-airfoil angle of attack. A large change in the direction of the wake-region velocity vectors with rotor loading occurs, seen by comparing the compressor and turbine forcing functions. The effect of the changing lift force direction is reflected by the large variation in the fundamental-harmonic β_w. The value of β_w changes from a value much greater than the linear-theory value, $\bar{\beta}_2 \approx 41$ deg, under compressor-loading conditions, $\beta_w = 101$ deg, to a value much less than the linear-theory value under turbine-loading conditions, $\beta_w = 6$ deg.

Figure 11 shows the effect of rotor solidity on the fundamental-harmonic linear-gust parameters of airfoil-cascade forcing functions. The rotor speed, i.e., inlet mean-relative flow angle, was constant. The difference between the gust-amplitude angle and the downstream mean-relative flow angle ($\beta_w - \bar{\beta}_2$) is plotted, with zero being the linear-theory value. The linear-gust parameters respond to rotor loading and rotor solidity with definite trends. On a vertical constant-rotor-solidity line ($\beta_w - \bar{\beta}_2$) is greatest with compressor loading, and decreases with neutral and turbine loading conditions. For similar loading conditions ($\beta_w - \bar{\beta}_2$) decreases with rotor solidity for the lower solidity values then increases at the higher-solidity values such that the data is near the linear-theory value, or showing the tendency of approaching the linear-theory value at the high-rotor-solidity values. The trends of the gust-component phase angles also show that increasing the rotor solidity tends to produce linear-theory results. Under neutral and turbine-loading conditions, ϕ_w decreases with rotor solidity to values below 180 deg, then increases to the linear-theory value at the intermediate-solidity values. Under neutral-loading conditions, ϕ_w correlates well with linear theory for rotor solidities above 0.35. Under compressor-loading conditions, ϕ_w decreases uniformly with solidity until the linear-theory value is reached at the higher-rotor-solidity values. Thus, high-solidity rotors tend to generate linear-theory vortical gust velocity profiles.

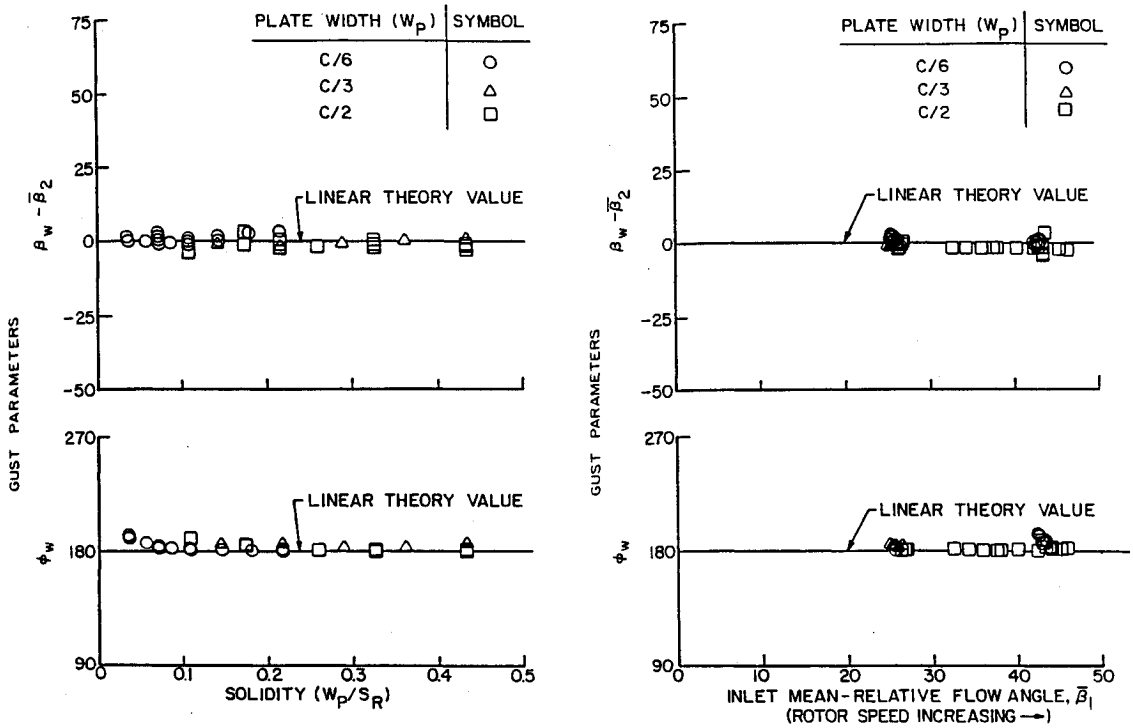

Fig. 7 Solidity and rotor speed effect on first harmonic perforated plate linear gust parameters.

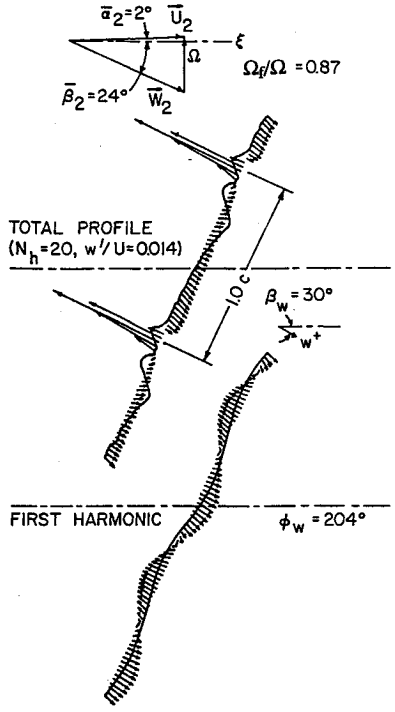

Fig. 8 Compressor loading effect on airfoil forcing function.

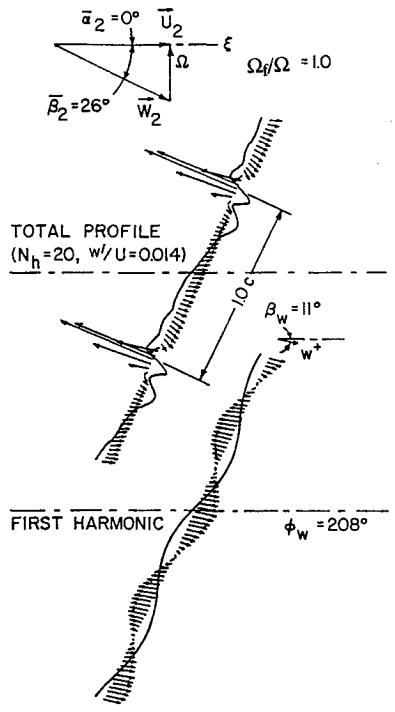

Fig. 9 Neutral loading effect on airfoil forcing function.

Stator Row Response—Linear Theory Gust

The response of the symmetric-airfoil cascade to perforated-plate forcing functions is presented in Fig. 12 in terms of the fundamental-harmonic unsteady lift and quarter-chord moment coefficients. The correlation with linear-theory is very good in both the subresonant and superresonant regimes away from the acoustic resonance. Near the acoustic resonance no evidence of the discontinuity predicted by linear theory is evident. The response data connect the subresonant regime with the superresonant regime by a simple linear trend. Thus, the acoustic resonance has little effect upon the airfoil unsteady loading.

Evidence of the acoustic resonance is clearly seen, however, in the chordwise surface responses (Fig. 13). In the subresonant regime the surface responses are similar to the results of the low-solidity symmetric-airfoil cascade experiments. The lower-surface response magnitude decreases monotonically from the leading edge to the trailing edge. The upper-surface response magnitude decreases rapidly over the front quarter chord, and a dip in the data trend is evident near the quarter chord. Near the trailing edge the response magnitudes are

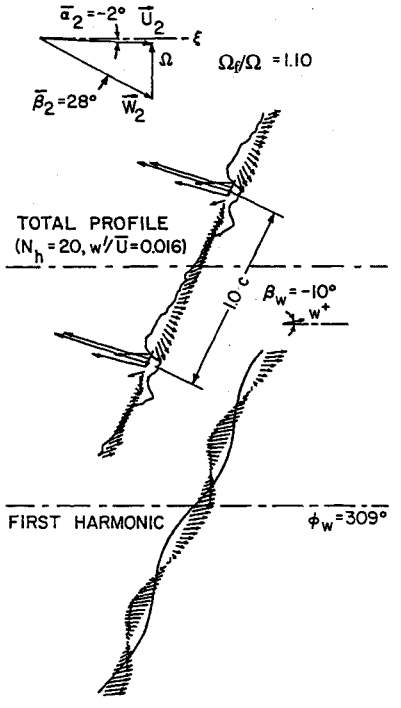

Fig. 10 Turbine loading effect on airfoil forcing function.

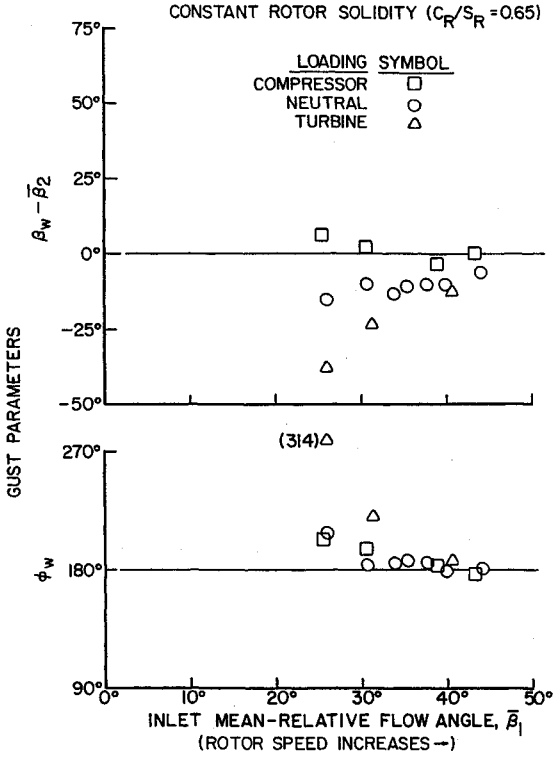

Fig. 11 Rotor loading and solidity effect on airfoil first harmonic linear gust parameters.

small. Near the leading edge the response phase angles are approximately 180-deg apart and in phase near the trailing edge.

The acoustic resonance condition was found by maximizing the unsteady surface pressures at the midchord by adjusting the rotor speed. Dramatically different airfoil surface responses result at resonance. At resonance, the upper-surface response magnitude dramatically increases from the subresonant levels over the entire chord except near the leading edge. The lower-surface response magnitude decreases greatly near the leading edge, and increases greatly near the trailing edge so that the trailing-edge magnitude is higher than the

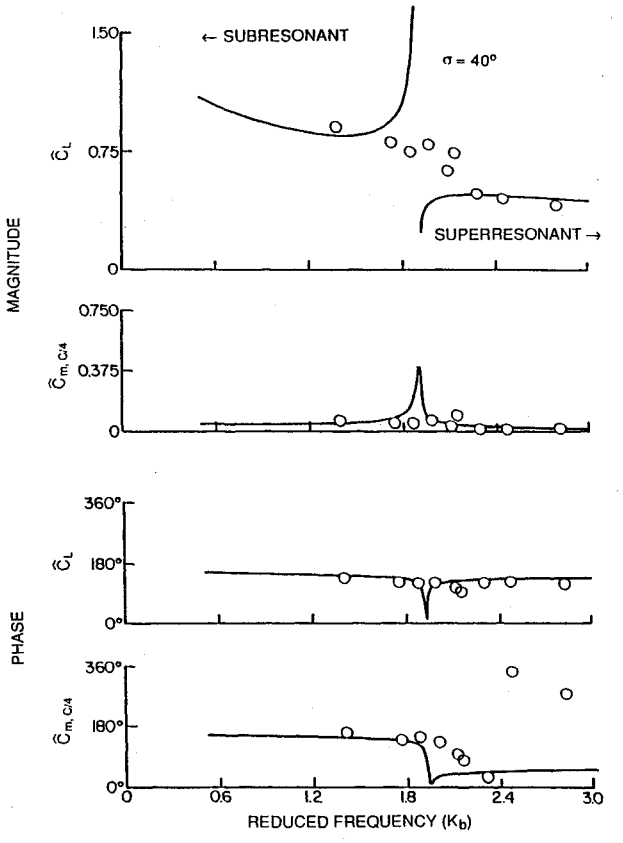

Fig. 12 First harmonic lift and moment coefficients—perforated plate forcing functions.

leading-edge magnitude. The phase angles of each surface merge toward the same value and the chordwise trend is very flat. Thus, the propagating pressure waves arrive along the chord at approximately the same time. In the superresonant regime the surface response magnitudes return to decreasing trends and the leading-edge response magnitudes are greater than the trailing-edge response magnitudes. The response phase angles near the leading edge are once again 180-deg apart.

Stator Row Response—Airfoil Wake Gust

The response of the symmetric-airfoil stator vane cascade to airfoil-cascade forcing functions is demonstrated in terms of the unsteady fundamental-harmonic lift and quarter-chord moment coefficients in Fig. 14. The rotor solidity was held constant and the reduced frequency was increased by increasing the rotor speed. The linear theory gust parameters are given in Fig. 11.

The unsteady aerodynamic coefficients are a strong function of rotor loading at the lower reduced frequencies, demonstrated by the large variations in the responses. The coefficients are weak functions of rotor loading at the higher reduced frequencies and tend to merge to the linear-theory prediction as the reduced frequency is increased. The linear-gust parameters are widely scattered at the lower rotor speeds and merge to the linear-theory values as the rotor speed is increased. Thus, the responses are tied to the behavior of the linear-gust parameters. Still, it is unclear how to use linear-gust parameters which deviate from the theory as a tool to predict the response.

The stator cascade responses show definite trends based upon the rotor-loading conditions which are reflected in the $(\beta_w - \bar{\beta}_2)$ values. For constant reduced-frequency values above the lowest value, the response increases as the rotor-loading changes from compressor to turbine conditions. This pattern corresponding to the forcing function results shows $(\beta_w - \bar{\beta}_2)$ values decreasing as the rotor-loading changes from compressor to turbine conditions. At the lowest reduced fre-

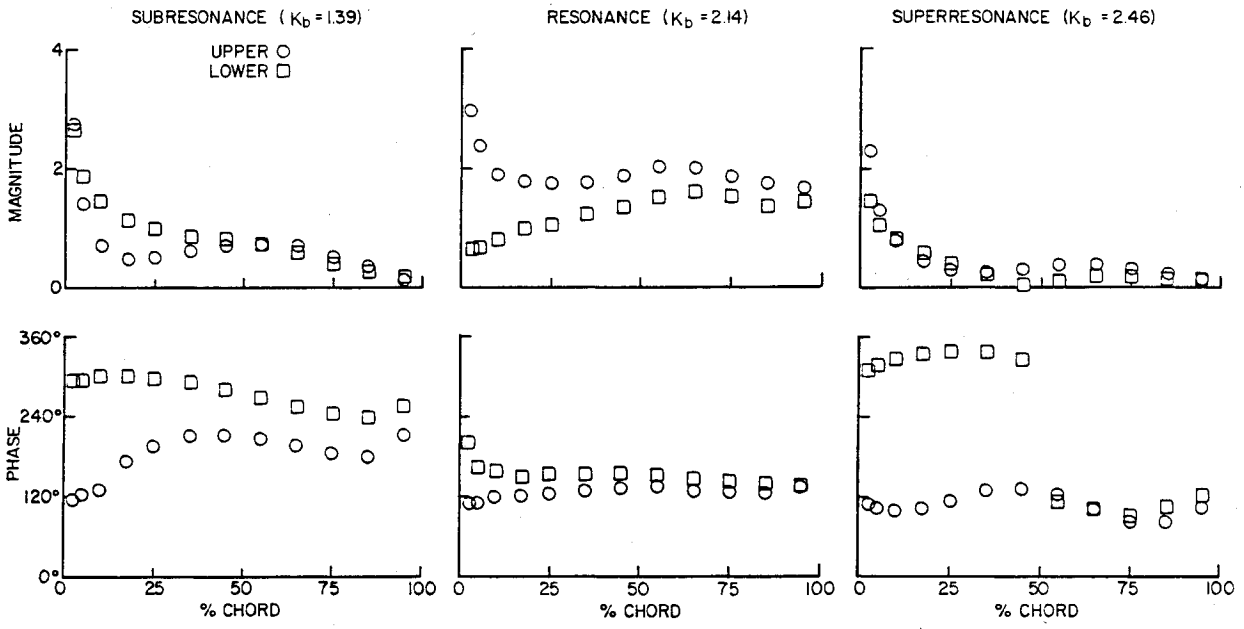

Fig. 13 Acoustic resonance effect on chordwise surface response—perforated plate forcing function.

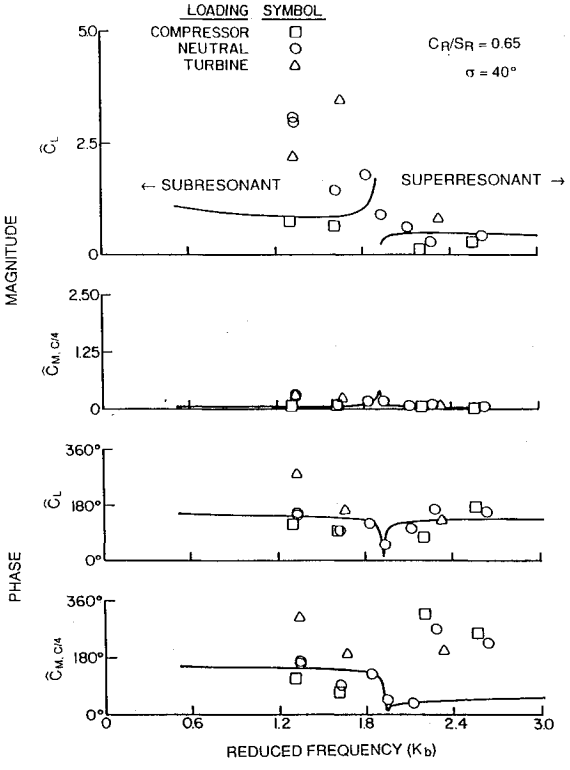

Fig. 14 First harmonic lift and moment coefficients—airfoil forcing functions.

quency, the neutral response is greater than the turbine response. This break in the response behavior due to rotor-loading may be tied to the much higher gust-component phase angle for the turbine case. Above the lowest reduced frequency, the compressor, neutral, and turbine gust-component phase angles are similar, and the predominant trend of the response increasing as the rotor-loading changes from compressor to turbine conditions is recovered.

The effect of rotor-loading condition on the chordwise unsteady pressure response of the stator cascade is presented in Fig. 15 for a subresonant reduced frequency (i.e., the lowest reduced frequency of Fig. 14). The upper-surface response magnitude trends are similar for neutral and turbine loading conditions over the leading half-chord. The response magnitudes decrease from the leading edge to 17% chord, then increase slightly to the midchord. Under compressor loading conditions the upper-surface response magnitudes decrease from the leading edge to the 35% chord, then increase slightly to 65% chord. Over the aft quarter chord the magnitude response trends are a function of the rotor-loading condition. Note the large increase in the upper-surface response magnitude at the 65% chord location when the rotor loading is changed from compressor to neutral conditions. The neutral and turbine-loading upper-surface response phase angles exhibit very similar trends, but the turbine response phase angles are shifted upwards by 120 deg. The compressor-loading response phase angles decrease slightly near the leading edge, whereas the neutral and turbine-loading response phase angles increase slightly near the leading edge. The upper-surface response phase angles are flat near the midchord. Near the trailing edge the response phase angles increase with chord position.

The lower-surface response trends are very similar for all rotor-loading conditions. The response magnitudes decrease rapidly from the leading edge to the 17% chord, then increase slightly to the midchord. Over the aft quarter chord the response magnitude trends are a function of rotor-loading conditions. The lower-surface response phase angles are weak functions of chord position from the leading edge to the midchord. Over the aft half chord, the response phase angle trends are a function of rotor loading conditions. The upper and lower-surface response phase angles are approximately 180-deg apart at the leading edge, and approximately in phase near the trailing edge.

Rotor loading affects the response of each surface. The upper-surface response magnitude increases greatly near the leading edge, remains relatively constant near the 17% chord position, and increases near the midchord as the rotor loading changes from compressor to neutral conditions. The response magnitudes decrease slightly from the neutral values when turbine-loading conditions are considered. The increase in the response magnitudes due to rotor-loading affects a larger portion of the chord on the lower-surface. The response magnitudes increase greatly from compressor to neutral-loading conditions, then decrease slightly for turbine-loading conditions. Changing the rotor loading from neutral conditions to turbine conditions shifts the response phase angles of each surface upwards by approximately 120 deg. The upper and lower-surface response magnitudes and phase angles are approximately equal near the trailing edge.

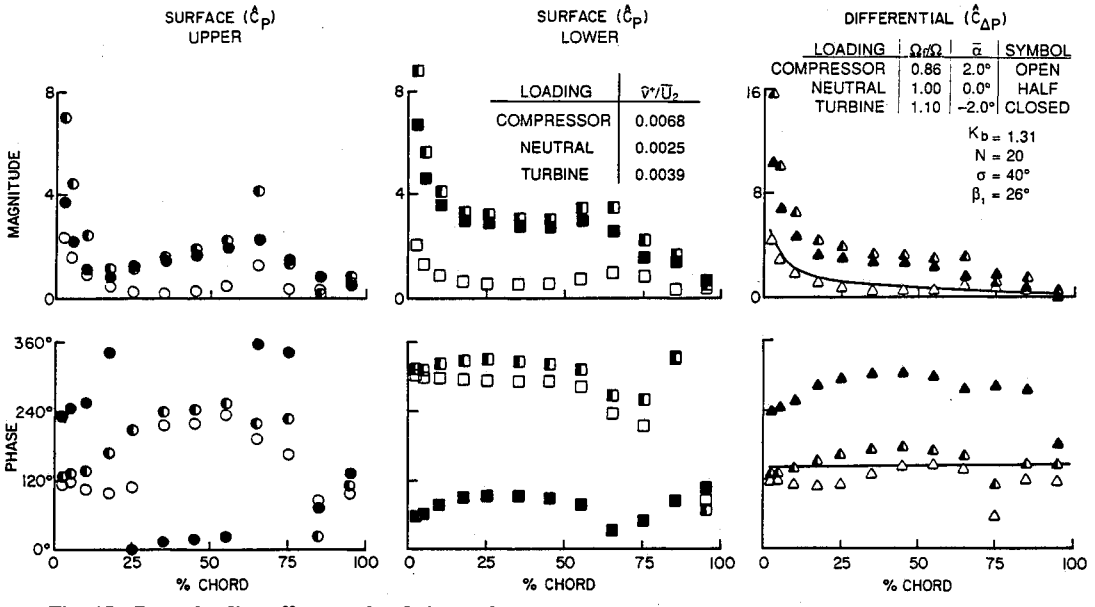

Fig. 15 Rotor loading effect on chordwise surface response—subresonant airfoil cascade forcing function.

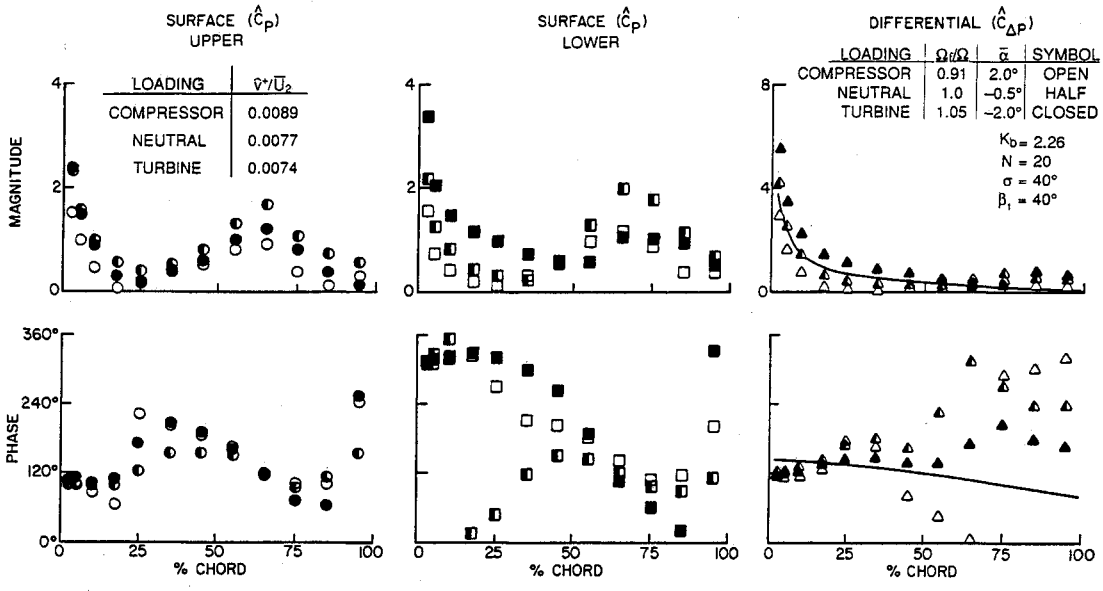

Fig. 16 Rotor loading effect on chordwise surface response—superresonant airfoil cascade forcing function.

The unsteady differential-pressure-coefficient magnitudes follow the general behavior of the predictions, but are a function of rotor-loading conditions. Under compressor-loading conditions, the unsteady differential-pressure-coefficient magnitudes are the lowest. A dramatic increase occurs for neutral loading, followed by a slight decrease under turbine-loading conditions. The behavior of the unsteady differential pressure coefficients is dominated by the response of the lower surface to the rotor-loading condition. The unsteady differential-pressure-coefficient phase angles are relatively weak functions of chordwise position, but strong functions of rotor-loading, demonstrated by the drastic increase in unsteady differential-pressure-coefficient phase angle under turbine-loading conditions.

The effect of rotor loading on the chordwise unsteady pressure response of the stator cascade is presented in Fig. 16 for a superresonant reduced frequency. The upper-surface response magnitudes exhibit similar sinuous chordwise trends which are large at the leading edge and 65% chord and small at the quarter chord and trailing edge. The upper-surface response phase angles are approximately equal near the leading edge. The response phase angles increase near the quarter chord with the increase greatest for rotor compressor loading. The response phase angles then decrease with chord to the 75% chord and then increase.

The lower-surface response magnitude trends are similar for compressor and neutral loading, and are approximately equal to the upper-surface values. The dip at the quarter chord, evident in the compressor and neutral-loading responses, is not present in the turbine-loading response. The lower-surface phase angles are approximately equal at the leading edge and approximately 180 deg out of phase with the upper-surface values. From the quarter chord to the midchord the response phase angle trends are functions of the rotor-loading condition. From the midchord to 75% chord the response phase angles are approximately equal and decrease with chord. Over the aft quarter chord the response phase angle trend is a function of rotor loading.

The upper-surface response magnitudes are relatively weak functions of rotor loading over the leading half chord. Over the aft half chord, the response magnitudes are stronger functions of rotor loading. The lower-surface response magnitudes are greater functions of rotor loading over the entire chord as compared to the upper surface. From the quarter chord to the midchord the response phase angles are strong functions of rotor loading on both surfaces.

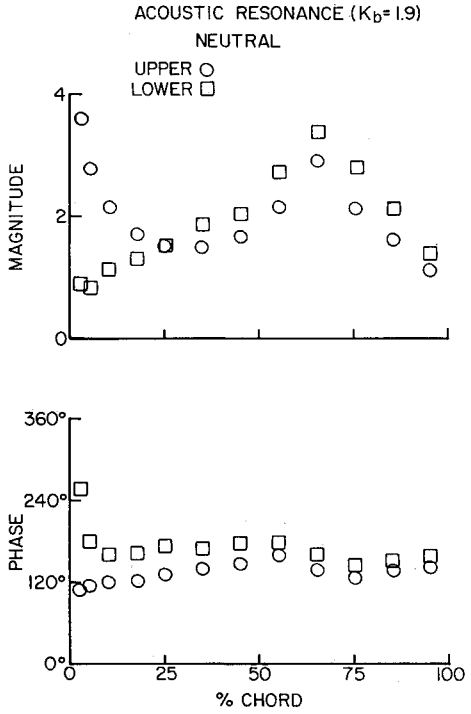

Fig. 17 Chordwise surface response near an acoustic resonance—airfoil cascade forcing function.

The unsteady differential-pressure-coefficient magnitudes follow the general trend of the linear-theory prediction, but increase as the rotor loading changes from compressor to turbine conditions. The compressor-loading unsteady differential-pressure-coefficient magnitudes display a relative minima at the quarter chord not predicted by the theory. The unsteady differential-pressure-coefficient phase angles vary widely as a function of rotor-loading condition over the aft half chord, even though the surface response phase angles are relatively weak functions of rotor loading from the midchord to the 75% chord. Note that the upper and lower surface responses are approximately equal in magnitude and in phase from the midchord to 75% chord. The large variations in the differential pressure coefficient phase angles result from small differences in the surface response magnitudes when surface response magnitudes and phase angles are approximately equal.

The effect of the acoustic resonance condition is strongly evident in the airfoil-cascade-generated surface response data of the stator cascade experiments. The subresonant and superresonant regime surface responses were presented in Figs. 15 and 16, respectively, with the surface response data very near the acoustic resonance presented in Fig. 17. The trends are similar to the perforated-plate-generated responses. In the subresonant regime, the leading-edge surface response magnitudes are high and the trailing-edge surface response magnitudes are small. The surface response phase angles are 180 deg out of phase near the leading edge, and in phase near the trailing edge. At the acoustic resonance condition, the lower-surface response magnitude decreases from the subresonant values near the leading edge and now increases with chord position. The surface response magnitudes increase greatly at the trailing edge so that the lower-surface response magnitude is larger at the trailing edge than at the leading edge. The upper and lower-surface phase angles become flat in the acoustic resonance results and merge toward a common value over the entire chord except near the leading edge. In the superresonant results (Fig. 16), the surface response magnitudes return to large values at the leading edge and low values at the trailing edge. The surface response phase angles diverge to values 180-deg apart near the leading edge, and are once again functions of chord position.

Summary and Conclusions

The unsteady aerodynamic gust response of a high solidity stator vane row, including the effects of operating in the subresonant and superresonant flow regimes, i.e., acoustic resonances, have been investigated experimentally in terms of the fundamental gust modeling assumptions for the first time. This was accomplished by means of a series of experiments performed in the Purdue Annular Cascade Research Facility. Linear theory gust forcing functions were generated by a rotating row of perforated plates, with the compressor and turbine blade wakes associated with a rotor blade row. The stator vane row was comprised of instrumented symmetric airfoils.

The perforated-plate forcing functions closely resemble linear-theory vortical gust forcing functions, with the static pressure fluctuations small and the periodic velocity vectors parallel to the downstream mean-relative flow angle over the entire periodic cycle. Unfortunately for the turbomachine designer, airfoil-cascade forcing functions are much more complex and exhibit characteristics far from linear-theory vortical gusts.

The response of the stator vane row to the linear theory vortical gusts generated by the perforated-plate forcing function pressure responses are in excellent agreement with linear theory predictions for experimental conditions not in the immediate neighborhood of an acoustic resonance. The unsteady pressure response correlation is consistent with the excellent correlation of the linear-gust parameters. The pressure responses do not agree with the linear-theory predictions near an acoustic resonance, but the effects of the acoustic resonance phenomena are clearly evident on the airfoil surface unsteady pressure responses. The transition of the measured lift coefficients from the subresonant regime to the superresonant regime occurs in a simple linear fashion. Thus, linear theory unsteady load predictions of a discontinuity between the subresonant and superresonant regimes are not valid.

The response of the stator vane cascade to airfoil-cascade forcing functions correlates poorly with linear-theory vortical gust predictions. The poor response correlations correspond to the poor linear-gust parameter correlations and high static pressure fluctuations, but no clear trend emerges which relates the linear-gust parameter values to the unsteady pressure response values. No effect of acoustic resonances were demonstrated in the airfoil-cascade-generated unsteady lift and moment coefficients, consistent with the perforated-plate generated coefficients. The unsteady lift and moment coefficients were controlled by the characteristics of the forcing function. However, the surface responses were obviously affected by the acoustic resonance and exhibited behavior similar to the perforated-plate-generated responses.

Acknowledgments

This research is sponsored, in part, by the NASA Lewis Research Center. Support, both financial and technical, for this research is most gratefully acknowledged.

References

[1]Scott, J. S., and Atassi, H. M., "Numerical Solutions of the Linearized Euler Equations for Unsteady Vortical Flows Around Lifting Airfoils," AIAA Paper 90-0694, Jan. 1990.

[2]Hall, K. C., and Verdon, J. M., "Gust Response Analysis for Cascades Operating in Nonuniform Mean Flows," AGARD Conf.—Unsteady Aerodynamic Phenomena in Turbomachines, AGARD CPP-468, 1989.

[3]Fang, J., "Compressible Flows with Vortical Disturbances Around Cascades of Airfoils," Ph.D. Dissertation, Univ. of Notre Dame, Notre Dame, IN, April 1991.

[4]Franke, G. F., and Henderson, R. E., "Unsteady Stator Response to Upstream Rotor Wakes," *Journal of Aircraft*, Vol. 17, No. 7, 1980, pp. 500–506.

[5]Fleeter, S., Jay, R. L., and Bennett, W. A., "Rotor Wake Generated Unsteady Aerodynamic Response of a Compressor Stator," *Journal of Engineering for Power*, Vol. 100, No. 4, 1978, pp. 664–675.

[6]Fleeter, S., Jay, R. L., and Bennett, W. A., "The Time-Variant Aerodynamic Response of a Stator Row Including the Effects of Airfoil Camber," *Journal of Engineering for Power*, Vol. 102, No. 2, 1980, pp. 334–343.

[7]Fleeter, S., Jay, R. L., and Bennett, W. A., "Wake Induced Time-Variant Aerodynamics Including Rotor-Stator Axial Spacing Effects," *Journal of Fluids Engineering*, Vol. 103, No. 1, 1981, pp. 59–66.

[8]Capece, V. R., and Fleeter, S., "Unsteady Aerodynamic Interactions in a Multi-Stage Compressor," *Journal of Turbomachinery*, Vol. 109, No. 3, 1987, pp. 420–428.

[9]Capece, V. R., and Fleeter, S., "Experimental Investigation of Multistage Interaction Gust Aerodynamics," *Journal of Turbomachinery*, Vol. 111, No. 4, 1989, pp. 409–417.

[10]Manwaring, S. R., and Fleeter, S., "Forcing Function Effects on Rotor Periodic Aerodynamic Response," *Journal of Turbomachinery*, Vol. 113, No. 2, 1991, pp. 312–319.

[11]Kim, K. H., and Fleeter, S., "Compressor Blade Gust Response to Attached & Separated Flow Forcing Functions," Sixth International Symposium on Unsteady Aerodynamics, Aeroelasticity and Aeroacoustics of Turbomachines and Propellers, Notre Dame, Notre Dame, IN, Sept. 1991.

[12]Henderson, G. H., and Fleeter, S., "Forcing Function Effects on Unsteady Aerodynamic Gust Response, Part I: Forcing Functions," American Society of Mechanical Engineers Paper 92-GJ-174, June 1992.

[13]Henderson, G. H., and Fleeter, S., "Forcing Function Effects on Unsteady Aerodynamic Gust Response, Part II: Low Solidity Airfoil Row Response," American Society of Mechanical Engineers Paper 92-GJ-175, June 1992.

[14]Goldstein, M. E., "Unsteady Vortical and Entropic Distortions of Potential Flows Round Arbitrary Obstacles," *Journal of Fluid Mechanics*, Vol. 89, Pt. 3, 1978, pp. 433–468.

[15]Carta, F. O., "Aeroelasticity and Unsteady Aerodynamics," *The Aerothermodynamics of Aircraft Gas Turbine Engines*, Air Force Aero Propulsion Lab. TR-78-521978, Chap. 22.

[16]Smith, S. N., "Discrete Frequency Sound Generation in Axial Flow Turbomachines," Aeronautical Research Council, R&M 3709, England, UK, 1972.